Plasma production from helicon waves

A. W. Degeling, C. O. Jung,[a] R. W. Boswell, and A. R. Ellingboe[b]
Space Plasma & Plasma Processing Group, Plasma Research Laboratory, Research School of Physical Sciences and Engineering, Australian National University, Canberra, Australia

(Received 13 October 1995; accepted 15 March 1996)

Experimental measurements taken in a large magnetoplasma show that a simple double half-turn antenna will excite $m=1$ helicon waves with wavelengths from 10–60 cm. Increased ionization in the center of the downstream plasma is measured when the axial wavelength of the helicon wave becomes less than the characteristic length of the system, typically 50–100 cm. A sharp maximum in the plasma density downstream from the source is measured for a magnetic field of 50 G, where the helicon wave phase velocity is about 3×10^8 cm s^{-1}. Transport of energy away from the source to the downstream region must occur to create the hot electrons needed for the increased ionization. A simple model shows that electrons in a Maxwellian distribution most likely to ionize for these experimental conditions also have a velocity of around 3×10^8 cm s^{-1}. This strong correlation suggests that the helicon wave is trapping electrons in the Maxwellian distribution with velocities somewhat slower than the wave and accelerating them into a quasibeam with velocity somewhat faster than the wave. The nonlinear increase in central density downstream as the power is increased for helicon waves with phase velocities close to the optimum electron velocity for ionization lends support to this idea. © *1996 American Institute of Physics*. [S1070-664X(96)03306-X]

I. INTRODUCTION

It has been known for a considerable time that helicon waves are associated with very efficient plasma production[1–5] and perturbations in the electron distribution function have been measured, which correlate with the helicon wave velocity.[4,6,7] Collisionless mechanisms such as Čerenkov damping.[8] Landau damping,[3] and Doppler shifted cyclotron damping[9] have been invoked to explain the high damping of the helicon wave. For the latter, very high densities are required to obtain the necessary Doppler shift and for most published laboratory experiments, the Landau or Čerenkov mechanism seems most likely.

However, applying the simple formulation of Landau damping for experimental wave velocities only a factor of 3 higher than the electron thermal velocity results in negligible damping.[4,8] Although the general picture of wave particle resonance seems to be correct, the details of the interaction would require solving the motion of the electrons trapped in the spatially varying wave fields. An added complication is the separation of the local interaction of the antenna fields with the plasma, and the remote traveling wave–particle interaction. The former can produce dense plasmas in the source by simple inductive coupling (although this is complicated by the presence of an axial magnetic field), or by generating axial standing helicon waves with a wavelength determined by the antenna length, the distance of the antenna from an endplate, i.e. by the radiated wave number spectrum of the antenna. The remote traveling wave–particle interaction tends to create dense plasmas downstream from the antenna in addition to the dense source plasma.[5]

For higher pressures, above 10 mTorr or so, or plasma densities above 10^{13} cm^{-3} (typically for helicon plasmas confined by magnetic fields above 500 G, where the wave frequency is close to the lower hybrid frequency), collisional damping of the helicon wave dominates collisionless damping and the electron collision frequency becomes much greater than the wave frequency, allowing a simple transfer of the oscillating field energy to the electrons. Under these circumstances, it is unlikely that electron beams resonant with the wave would be seen. In the present paper we are concerned with pressures less than 5 mTorr, low magnetic fields around 50 G, and plasma densities up to 5×10^{11} cm^{-3}.

II. EXPERIMENTAL DESCRIPTION

The large plasma diffusion system WOMBAT[10] (Waves On Magnetized Beams And Turbulence) consists of a glass source tube 50 cm long and 18 cm in diameter, attached on axis to a large stainless steel diffusion chamber 200 cm long and 90 cm in diameter, as shown in Fig. 1. The other end of the source is terminated by an aluminum plate through which various probes can be inserted. A steady axial magnetic field is provided by a set of external solenoids surrounding the source and a large solenoid inside the diffusion chamber. As a rule, the magnetic field on axis in the source is set to be twice the value in the diffusion chamber. This ensures that the field decreases monotonically when going from the source to the diffusion chamber. This is also a situation commonly found in high-density diffusion plasma processing reactors.

A base pressure of 10^{-6} Torr can be maintained by a Balzers turbo pump with a pumping speed of 330 L/s connected to the diffusion chamber on the end opposite the source. Operating pressures of between 0.5 and 3 mTorr of argon are set by adjusting the flow rate of gas using a needle valve on the gas feedline. The pressure (in the milliTorr range) is measured using a baratron pressure gauge, and the flow rate in sccm by a flow meter.

[a]Also at Samsung Electronics, Korea.
[b]Also at Lawrence Livermore National Laboratories, Livermore, California 94550.

 1070-664X/96/3(7)/2788/9/$10.00

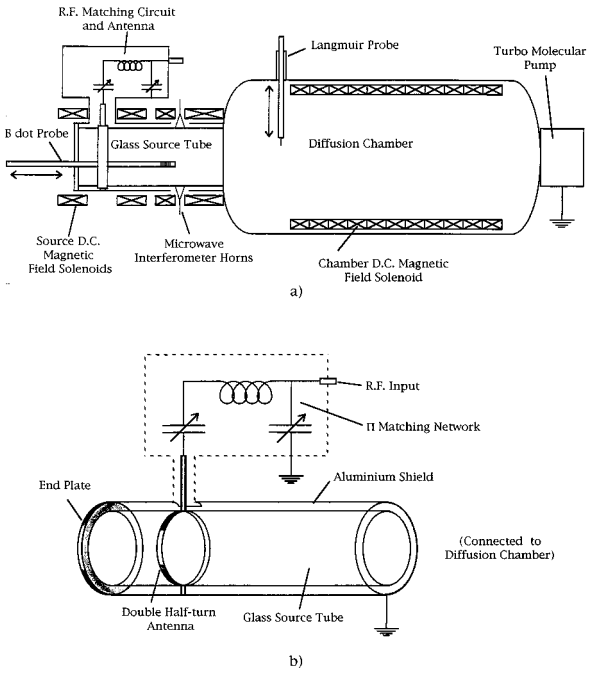

FIG. 1. (a) Experimental layout of the WOMBAT apparatus. (b) Electrical circuit of the match box and double half-turn antenna.

A rf (radio frequency) power supply provides up to 2.6 kW of forward power at a frequency of 13.56 MHz to the Pi network matching circuit and antenna. The antenna used in this experiment is situated around the glass source tube directly below the matching box. It consists of a single loop of copper (20 cm in diameter, 1 cm wide, and 0.3 cm thick) concentric with the axis of the source and situated 7.5 cm from the conducting end of the source. The antenna is connected to the output of the matching circuit at the top, and a grounded aluminum electric shield surrounding the vessel at the bottom, as shown in Fig. 1, and is known as a double half-turn antenna. This configuration couples into the $m=+1$ and -1 helicon modes (where m is the azimuthal mode number) in the plasma.[11] Because the inductance of the antenna is low at 0.2 mH, a rather large inductor of 1.4 mH is necessary in the match box, and heating of this circuit element is responsible for a high percentage of the resistive power loss.

III. PLASMA DIAGNOSTICS

A. Langmuir probe

A Langmuir probe is inserted radially into the diffusion chamber 112 cm from the source endplate. The probe consists of a flat circular tantalum disk of area A equal to 1.0 cm^2, which is oriented perpendicular to the axis of the vessel, and is coated with insulating material on the side facing away from the source. The voltage on the probe is set to -80 V using a floating dc (direct current) voltage supply. This voltage is chosen to be about 100 V less than the floating potential so that the current drawn to the probe can be assumed to be the true ion saturation current. The probe's radial position is adjustable, and allows radial profiles of the saturation current to be taken using an $X-Y$ recorder.

The plasma density at the position of the probe is estimated from the ion saturation current i_{sat} by considering the ion flux to the probe surface, given by

$$i_{sat}=0.6Ane\nu_B,$$

where the Bohm velocity ν_B is 4×10^5 cm/s for an electron temperature of 3 eV, which has been measured previously in WOMBAT under similar conditions.

The probe area is made deliberately large to ensure that the current collected when in ion saturation is insensitive to the probe voltage. This is because the size of the sheath is always much smaller than the probe dimensions, so variations in the sheath size due to changes in the probe potential do not significantly change the current collection area. We therefore expect rf modulation in the plasma potential to only have a negligible effect on the current measurements with this probe design.

B. Microwave interferometry

Two microwave interferometers are used in this experiment that operate at frequencies of 10 and 35 GHz, respectively. In each case the interferometer is positioned such that line density measurements are taken across a diameter in the source, 35 cm downstream from the antenna.

The line integrated density across the source tube, where L_p is 18 cm and λ_0 is 3 cm for 10 GHz microwaves and 0.8 cm for 35 GHz microwaves, is related to the phase shift $\Delta\phi$ due to the plasma by

$$n=n_{c0}\left[1-\left(1-\frac{\lambda_0\,\Delta\phi}{2\pi L_p}\right)^2\right].$$

It is assumed that the path of the microwaves through the plasma does not change with the density—that is the microwave beam is not refracted. This is equivalent to asserting that the plasma is axisymmetric in density, since the microwave beam is directed across the diameter of the source. This is reasonable for inductive and helicon wave coupled plasmas, however, capacitive plasmas are probably not axisymmetric since the voltage drops across the antenna.

Some of the measurements taken with the 10 GHz interferometer exhibit spurious fluctuations, which do not correlate with measurements using the 35 GHz interferometer, or the Langmuir probe measurements farther downstream. These fluctuations are thought to be due to standing waves set up in the cavity defined by the Earth shield surrounding the source tube. Figure 2 shows line density measurements from the 10 GHz interferometer against the input power for magnetic field settings of 25, 50, 100 and 150 G. The dashed line in these graphs is the square law best fit to this data, and indicates the general trend of the line density variation with increasing power in each case. Line density measurements from the 35 GHz interferometer are also shown in Fig. 2(b) (50 G), and exhibit the same general trend as the 10 GHz measurements.

C. Wave magnetic field probe (B-dot probe)

The rf magnetic field component in the axial direction (b_z) is measured using a magnetic field probe for various

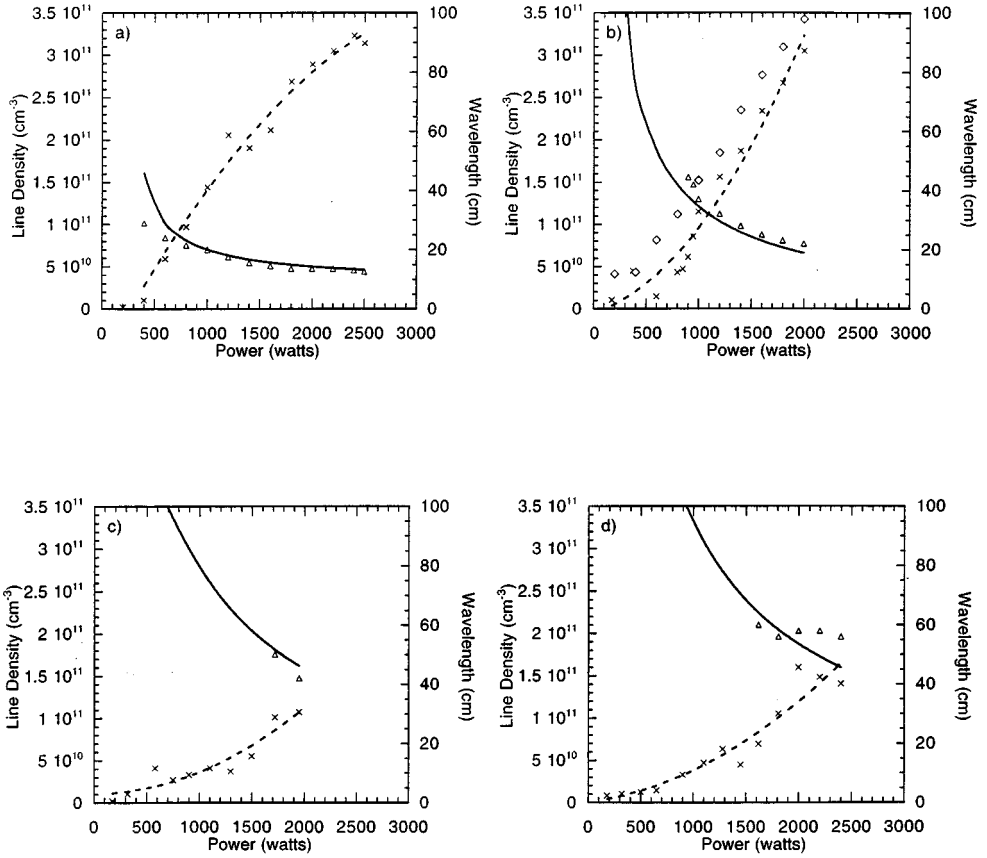

FIG. 2. Line density measured by the interferometers in the source and axial B-field wavelength as a function of power for 25, 50, 100, and 150 G.

plasma conditions. The probe consists of a five turn winding of thin copper wire around the end of a 0.6 cm diameter, 75 cm long cardboard tube, which is inserted axially into the plasma from the end of the source tube. The probe is separated from the plasma by a glass tube that is closed at the end. The glass tube is situated at a radius of 4 cm, where previous measurements have shown the B_z component of the helicon wave to have its maximum amplitude,[11] and extends fully through the source tube, allowing magnetic field measurements to be taken over this region. Since at high powers the glass tube is heated by the plasma, the probe is air cooled in order to prolong its life. The probe head is simply an inductor, and a rapidly changing magnetic flux perpendicular to the probe cross section generates a voltage across the ends of the winding. The probe also picks up the rf electric field from the plasma by electrostatic coupling. The electrostatic pickup gives rise to a common mode signal on the twisted pair connecting the probe to the output, whereas the magnetic pickup gives rise to a differential signal. These signals are separated using a hybrid combiner.[12] The output voltage is monitored on an oscilloscope in conjunction with the antenna current signal, which is used as a phase reference.

D. Wavelength measurements

It is expected that the rf magnetic field in the plasma would exhibit standing wave behavior when close to the antenna, and traveling wave behavior when farther away if the helicon mode was operating.[4] The B-dot probe measures the time variation of the rf magnetic field at a single point in space, so spatial standing waves and traveling waves may be diagnosed by observing how the amplitude and phase of the probe signal changes as the probe position is changed. For standing waves, the phase remains constant until the probe passes through half a stationary wavelength, at which point the phase changes by 180°, while the amplitude changes from maximum to minimum and back to maximum (for example) over the same distance. For traveling waves, the phase varies smoothly as the probe position is changed and the amplitude may or may not change depending on the attenuation of the wave. In this case one wavelength is measured by noting the distance the probe is moved to change the phase by 360° with respect to the reference signal.

The wavelength for traveling waves is measured using this method as a function of the input power for various magnetic field settings, and a gas pressure of 3 mTorr. Under some conditions the standing wave mode extends well away from the antenna, or the traveling wave wavelength is so long that only a half- or quarter-wavelength can be measured, if at all. In these cases the precision of the measurement is obviously degraded. The longest wavelength measurement made is 60 cm by measuring a quarter-wavelength. It is unclear whether traveling waves exist in the source with longer wavelengths, since the change in phase with the probe position becomes increasingly difficult to measure.

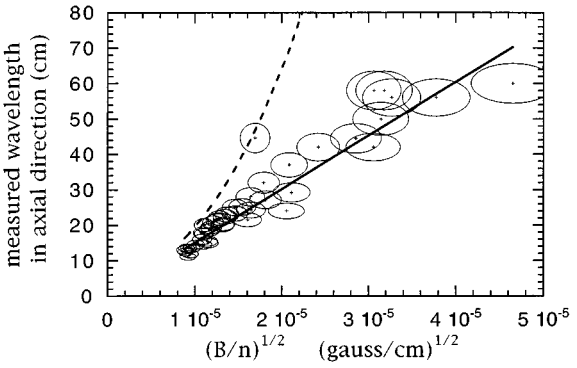

FIG. 3. Experimental measurements of wavelength against the root of the source magnetic field divided by the source line density. The solid line is the theoretical helicon wave dispersion relation for plane waves in an infinite plasma.

IV. RESULTS

A. Existence of helicon waves

In general, the results are taken for a given set of parameters as the rf power was increased. In order to determine the characteristics of the waves in the plasma and whether they are helicon waves, the B-dot probe is moved along the axis at a radius of 4 cm, where the $B_{\tilde{z}}$ component of the $m=1$ helicon wave has a maximum.[11] The phase of the signal is compared to the constant phase of the antenna current and a phase change of 2π defines one wavelength. At the same time the line density in the source is measured with either a 10 GHz or a 35 GHz interferometer. These measurements are plotted in Fig. 2 for source magnetic fields of 25, 50, 100, and 150 G. The square law best fit to the line density measurements (shown as a dashed line in each graph) is used to calculate the axial wavelength according to the simple plane wave dispersion relation for helicon waves in an infinite plasma, and is shown as the solid line in each graph.

The dispersion relation for helicon waves in a bounded system is

$$k_{\parallel}^4+k_{\perp}^2k_{\parallel}^2-\left(\frac{\mu_0 ne\omega}{B}\right)^2=0,$$

where ω is the wave frequency (in rad s^{-1}), B is the axial magnetic field, n is the plasma density, e is the electronic charge, μ_0 is the permittivity of vacuum, and the wave number has parallel and perpendicular components, $k^2=k_{\parallel}^2+k_{\perp}^2$. In a cylinder of radius r, $k_{\perp}$ is given by the zero of the first Bessel function $k_{\perp}=3.83/r$. Previous measurements in WOMBAT show that equal amounts of $m=+1$ and $m=-1$ modes are excited, as would be expected from the symmetry of the double half-turn antenna design. Hence the wave is essentially plane polarized.

The measurements of wavelength, line density, and source magnetic field are presented in Fig. 3, which shows the wavelength plotted against $(B/n)^{1/2}$. These data agree with the solution of the dispersion relation with $k_{\perp}=0$ (solid line) and clearly diverges from the solution with $k_{\perp}$ specified by the source radius of 9 cm (dashed line). It is expected that our data should fit a solution with $k_{\perp}$ specified by a radius of less than 9 cm, since the density is not uniform, as assumed in this calculation, but is strongly peaked toward the center. Such solutions lie to the left of the solution for 9 cm in Fig. 3, and diverge even more rapidly from our data. The reason for this behavior is not presently understood.

Two general trends can be seen in Fig. 2: the density has a maximum at 50 G, and a sharp increase in the density occurs as the helicon wavelength enters the source (around 50 cm). Both of these trends are exacerbated in the ion saturation measurements in the center and downstream from the source taken with the Langmuir probe shown in Fig. 4.

B. Mode transitions

For the higher magnetic fields, three types of density variation with input power can be discerned as the power is increased: an initial slow variation, followed by an increase and a saturation, and then a rapid increase continuing to the maximum power available (2.5 kW). We have named these three regions as the E, H, and W discharges and they correspond to capacitive, inductive and wave coupling.[11] As the magnetic field is decreased, the density necessary for maintaining a helicon wavelength in the source decreases, and at 25 G the plasma moves from the E discharge to the W discharge at a few watts without apparently going through a distinct H discharge region.

1. The E–H transition

The E–H transition occurs at a density of about 10^{10} cm^{-3}, independent of pressure and magnetic field, and seems to be related to the collisionless skin depth:

$$\delta=c/\omega_{pe},$$

where c is the speed of light and ω_{pe} is the electron plasma frequency (in rad s^{-1}). The reason for this is not known to us at present, although the E–H *transition*—generally occurs when δ is equal to about half a radius. It may be that for these conditions, the near field of the antenna is reduced by about an order of magnitude in the center of the plasma and anomalous cross-field diffusion driven by the asymmetric electric fields of the antenna is reduced.[13] It this is true, then the density can increase further, decreasing the skin depth, and a positive feedback will be developed, resulting in a sudden density increase. This type of phenomenon will also show considerable hysteresis as the power is increased and then decreased, supporting the notion that the skin depth is the determining parameter and not the antenna voltage or current.

2. The H–W transition

Below the transition, the radial density profiles are characterized by a hollow density profile with two distinct maxima or shoulders. The shoulder peaks map along the magnetic field lines to the radial periphery of the source and are typical of an inductive discharge.

Since the plasma is confined by the magnetic field, an increase in the plasma density will serve to decrease the skin depth and the plasma profile will show an increasingly deep minimum in the center when in the H mode, as the electric fields that accelerate the electrons are increasingly excluded.

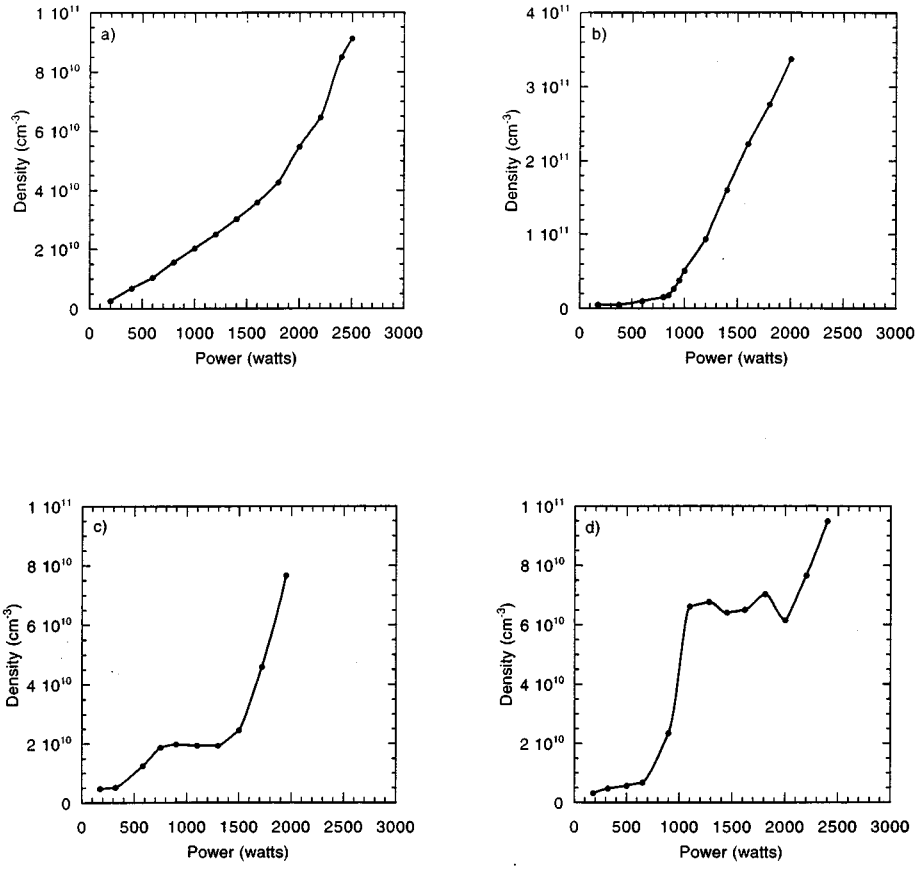

FIG. 4. Langmuir probe measurements of the central plasma density in the downstream region as a function of power for 25, 50, 100, and 150 G.

Above the transition, there appears a central maximum that increases as the power is further increased. The H–W transition is clearly evidenced by the appearance of traveling waves in the source, and is concurrent with the initiation of the increase in the central density. As this increase cannot be explained by the inductive coupling mechanism, another phenomenon must be responsible. Examples of the density profiles obtained from the ion saturation current of the Langmuir probe are shown in Fig. 5 for conditions before and after the transition for a source magnetic field of 150 G. A constant radial electron temperature has been assumed in calculating the density, which is probably justified along magnetic field lines connected to the source. Outside this region, the electron temperature may decrease (i.e., for radii greater than about 15 cm), and this effect would increase the density in the wings by possibly 50% compared to that shown in Fig. 5. Nevertheless, the overall form of the radial density variation would not change. The transition from the H to the W mode may be seen by an increase in the ratio of the center density to the shoulder density. This ratio is plotted in Fig. 6

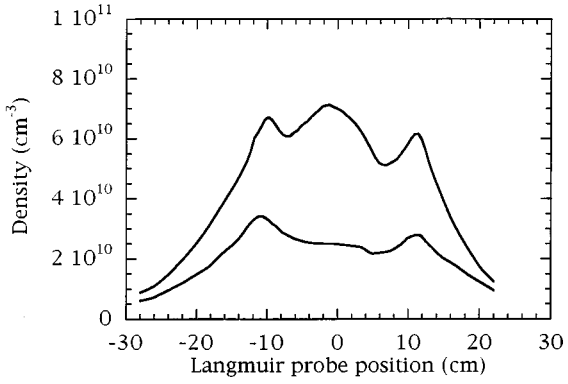

FIG. 5. Radial density profile in the downstream region at 150 G, taken with the Langmuir probe for 1000 and 2000 W.

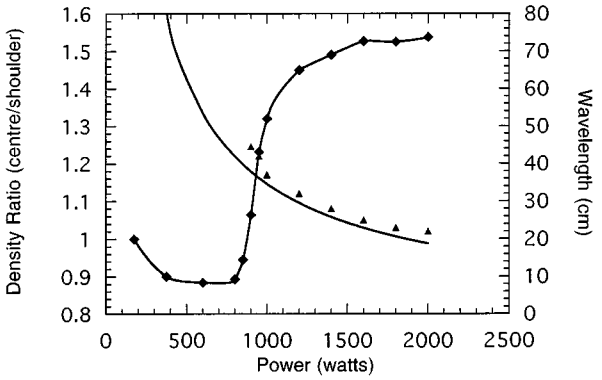

FIG. 6. Ratio of center to shoulder densities and helicon wavelength as a function of power for 50 G.

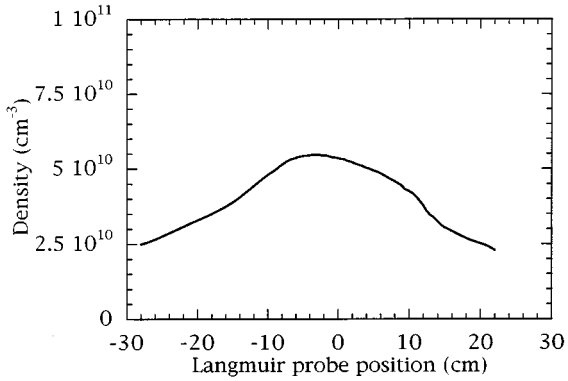

FIG. 7. Radial density profile in the downstream region taken with the Langmuir probe for 2000 W and 25 G.

as a function of power for the standard condition of 50 G, along with the traveling wavelength measurements. The correlation between the appearance of traveling helicon waves and plasma production downstream from the antenna in the center of the source suggests that the helicon wave is responsible for power input to the plasma; hence we label this regime of operation as the W mode.

As mentioned above, for lower magnetic fields, a lower density is required for the helicon wave to enter the system and the H–W transition occurs at a lower power. Consequently, helicon wave generated plasma dominates the plasma profile, as can be seen in Fig. 7, where there is little evidence of the H mode. Hence, depending on the magnetic field, for the same input rf power, the plasma can be completely inductive with a hollow profile or helicon wave generated with a centrally peaked profile.

C. Plasma production by helicon waves

The measurements of both Figs. 2 and 4 show a density maximum for a magnetic field of 50 G. Naively, one would expect the cross-field diffusion to decrease as the magnetic field increases, resulting in a consequent increase in the density. This is clearly not the case in this experiment, so the change in density must come from a change in the ionization efficiency. A further set of experiments were carried out for constant input rf power with a changing magnetic field. As the density peak was much more pronounced downstream, the ion saturation current of the Langmuir probe in the center of the plasma was measured rather than the interferometer measurement, which gives a line integral density across the plasma and would not be particularly sensitive to gradual increases in the central plasma density. These measurements are shown in Fig. 8. For input rf power less than 1000 W, there is no clear maximum; the decrease in density for low magnetic fields presumably being due to decreased diffusion from the source. For higher powers there is a very clear maximum at about 50 G that cannot be explained by simple diffusion of the plasma along the magnetic field lines from the source. In Fig. 8(b), measurements of the helicon wavelength made simultaneously with the Langmuir probe measurements at 2000 W are presented and show that there is

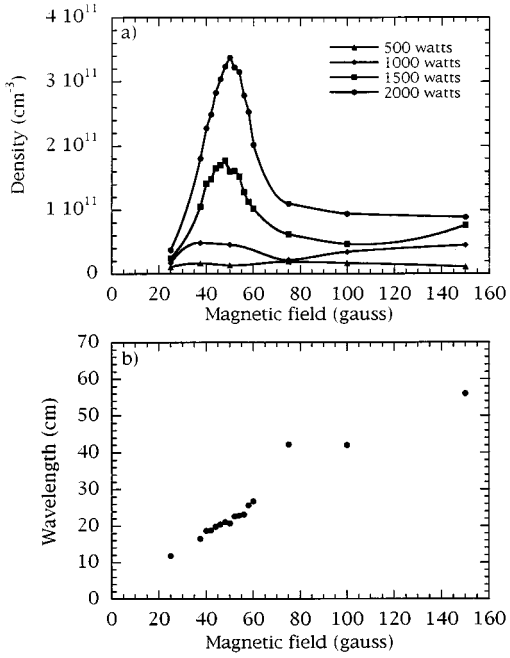

FIG. 8. (a) Downstream density in the center taken with the Langmuir probe for powers of 500, 1000, 1500, and 2000 W; and (b) wavelength measurements at a power of 2000 W, as a function of the source magnetic field.

always a helicon wave present in the system and its wavelength increases with the magnetic field. By multiplying the wavelength by the frequency of the rf generator (13.56 MHz) the phase velocity of the helicon wave parallel to the magnetic field can be determined, and Fig. 8 can be replotted to show the variation of the density as a function of this velocity. With the new ordinate, the density maximum appears in Fig. 10 at a phase velocity of around 3×10^8 cm s^{-1}.

D. Electrons in a Maxwellian distribution most likely to ionize

In order to gain some understanding of how the helicon waves can contribute to the efficient ionization of the plasma, it is necessary to determine which electrons in a Maxwellian distribution contribute most to the ionization in the present experiment and whether helicon waves can interact with these electrons. In Fig. 9 are plotted a normalized 3 eV Maxwellian distribution for the electrons, the ionization rate for argon, and the mean-free path for ionizing collisions (λ) at 3 mTorr, all as a function of electron velocity. For the present paper, we are interested in finding a simple explanation of the efficient ionization by helicon waves so only ionizing collisions will be considered, although elastic collisions with neutrals will modify the results slightly. As mentioned previously, helicon waves seem to interact resonantly with only a specific group of electrons and not with the bulk of the Maxwellian distribution. Therefore, we multiply the curves given in Figs. 9(a) and 9(b) to obtain Fig. 9(c), which represents the electrons most likely to ionize in the 3 eV Maxwellian. However, the finite length of the experiment must be taken into account, so the likelihood of these electrons making an ionizing collision in a system of length (L =50 cm) must be included. This is achieved by multiplying

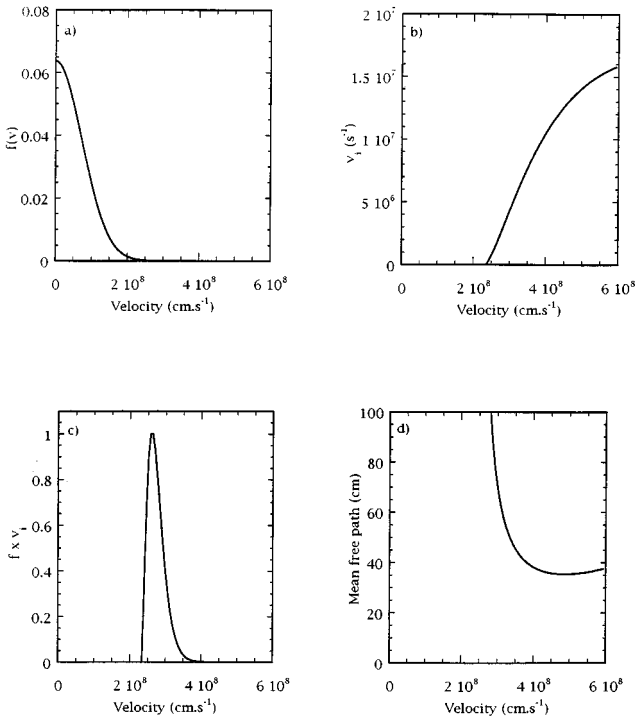

FIG. 9. (a) 3 eV electron distribution function. (b) Ionization rate for argon; (c) previous two curves multiplied together to show which electrons in the distribution are most effective in ionizing; (d) mean-free path for ionizing collisions, plotted against velocity.

Fig. 9(c) by the factor $1-\exp(-L/2)$ and the resulting curve shown in Fig. 10. The experimental measurements derived from Fig. 8 are also plotted to allow a direct comparison to be made. There is a high correlation between the position of

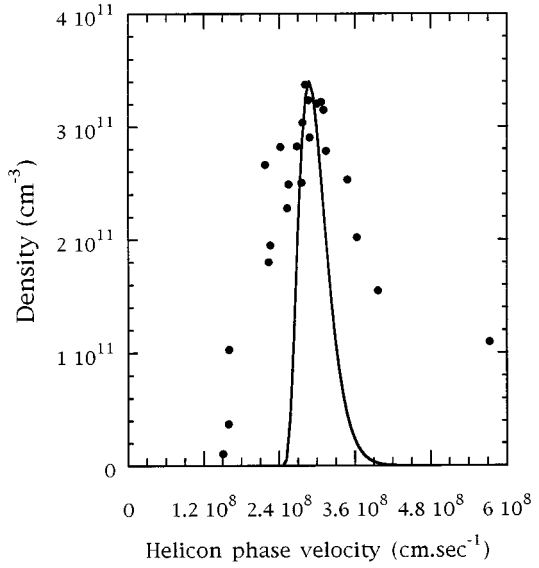

FIG. 10. Experimental density measurements from Fig. 8(a) plotted against the helicon phase velocity determined from Fig. 8(b) for a power of 2000 W compared with a curve showing the electrons most likely to ionize in the length of the source.

the two maxima which strongly suggests that the helicon is trapping electrons from the Maxwellian distribution and accelerating them to higher velocities.

Direct evidence of significant numbers of electrons accelerated to the wave phase velocity has been observed previously on WOMBAT over an axial distance of 40 cm for argon at 3 mTorr by Ellingboe *et al*. (using optical emission spectroscopy resolved in time to one-tenth of an rf period).[4] In that experiment, the excitation of argon ions by the electron beam gives rise to bursts of emission that propagate away from the antenna at the wave phase velocity. The intensity of the observed emission demonstrates that the collision frequency of electrons from the beam with ions is significant (although not high enough to preclude the formation of the beam). The mean-free path for momentum transfer collisions of 30 eV electrons with neutrals is 10–15 cm, i.e. the same order as the helicon wavelength. The combined effects of inelastic and elastic collisions would serve to scatter a large proportion of the trapped electrons out of the wave frame before they complete of a full bounce period and return energy to the wave.

In the present experiment, these accelerated electrons would give rise to a dramatic increase in the ionization rate (as well as the excitation rate measured previously under very similar conditions)[5] downstream from the antenna for conditions such that the phase velocity approaches the optimum velocity of 3×10^8 cm s^{-1}, which is the maximum of the ionization efficiency. To understand how this may occur, it is necessary to discuss the trapping of electrons by a large-amplitude wave.

V. DISCUSSION

A. Trapping model

Waves in plasmas that have a component of their electric field parallel to their direction of propagation can interact with electrons that have velocities close to the wave velocity. If the slope of the electron distribution function at this velocity is negative, the wave will damp and for small-amplitude waves with velocities not far from the electron thermal velocity, the damping decrement is given by the theory of Landau. The simple view is that the wave accelerates electrons with velocities slightly lower than the wave velocity to velocities slightly higher, and similarly decelerates electrons with velocities slightly higher than the wave to velocities slightly lower. As there are more electrons with velocities slightly lower, this interaction results in energy being taken from the wave that consequently damps. The damping of the wave ceases when a small plateau in the distribution function is formed around the wave velocity (i.e., the slope of the distribution function becomes zero). For large-amplitude waves, electrons are trapped in the wave fields. This can be visualized by moving into the wave frame where the wave is a static, approximately sinusoidal potential. Trapped electrons are accelerated down the potential, attain their maximum velocity at the potential minimum, and then decelerate as they climb the increasing potential. The motion near the bottom of the potential well can be described

as a form of simple harmonic motion in a potential trough with the trapped electrons having a trapping period:

$$\tau = 2\pi\left(\frac{m}{eE_z k}\right)^{1/2},$$

where m is the electron mass, e its charge, E_z the wave electric field amplitude, and k is the wave number. If τ becomes comparable to or less than the time scale for Landau damping the linear theory is no longer valid since the motion of the electrons in the trough of the wave effect the shape of the wave and the problem becomes severely nonlinear (further information on this topic can be found in the book by Davidson[14]). Particle in cell computer simulations of beam–plasma interactions and beam–plasma discharges are one of the main guides to understanding these complicated phenomena (see, e.g., Ref. 15). For the experiment described here, τ is well over an order of magnitude smaller than the time scale for Landau damping and so the Landau theory is not applicable, and we shall resort to a qualitative description in the hope that it can be tested experimentally.

The major difference between the simple wave–particle interaction, which occurs close to the electron plasma frequency, and the interaction of electrons with the helicon is that in the latter case, the wave frequency is in the megahertz range and in the former case in the gigahertz range. This results in longer wavelengths for helicon wave resonant interactions with the electrons, which are much easier to measure experimentally. Additionally, for our experimental conditions, the trapping length, the wavelength, and the mean-free path for electron collisions are comparable.[4]

Consequently, only the E_z component of the helicon will be considered, and the same concepts used as in electrostatic wave–particle interactions. Electrons trapped in the E_z fields of the wave have a trapping width in velocity space around the wave velocity of

$$v_t = \pm\left(\frac{eE_z}{mk}\right)^{1/2},$$

where m is the electron mass and we have allowed for poorly trapped electrons close to the separatrix by removing the 2 from the root.

Since we have shown earlier that it is very probable that the trapped electrons come from a Maxwellian distribution;

$$f(n) \sim \exp\left(-\frac{mv^2}{2T_e}\right),$$

where T_e is in eV, it can be shown after a certain amount of algebra (Dewar[16]) that the number of electrons trapped by the wave would increase exponentially with the square root of the wave amplitude (for a constant T_e):

$$n_t \sim \exp(E_z^{1/2}).$$

From the ANTENA[17,18] code we have noted a linear relation between E_z and the antenna current, as would be expected. For an ideal system we would then expect E_z to be proportional to the square root of power, and hence the density of trapped electrons:

$$n_t \sim \exp(\text{power}^{1/4}).$$

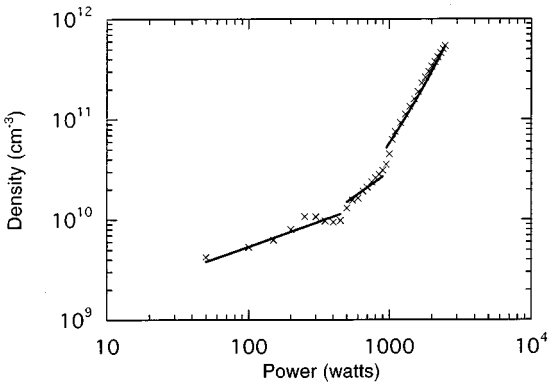

FIG. 11. Detailed Langmuir probe measurements of the central downstream density as a function of power. The three different modes can clearly be seen.

If the wave velocity is close to that necessary to accelerate electrons to the most effective ionizing velocity (i.e., around 3×10^8 cm s^{-1}) and if the plasma loss mechanisms remain constant, then an exponential increase in the ionization rate, and consequently the plasma density, would be expected as the power increases. To support this model we note that when a helicon wave is in the system the plasma density downstream increases faster than linear with power, whereas the plasma density in the source under the same conditions increases linearly with power. The variation of the central downstream density as a function of power for a source magnetic field of 50 G is plotted in more detail in Fig. 11. On this log–log plot the three discharge modes can be quite clearly distinguished. The low-power capacitive coupling shows a density variation close to the square root of power, the inductive coupling shows a near linear variation, and the helicon wave coupling shows an exponential variation. For the latter, the exponent of power in the exponential is 0.29, which is very close to the 0.25 predicted by our simple theory.

VI. CONCLUSIONS

A simple double half-turn antenna has been shown to excite $m=1$ helicon waves that are correlated with an increase in the central density of the plasma. A density maximum in the downstream plasma occurred for a wave phase velocity of 3×10^8 cm s^{-1}, which is the velocity of electrons in a Maxwellian distribution that are most effective in ionizing. The results are interpreted in terms of wave–particle trapping that predicts an exponential increase in the downstream density as the power is increased, which is consistent with the experimental measurements.

ACKNOWLEDGMENTS

The authors would like to thank A. J. Perry and G. D. Conway for their practical advice and experimental assistance, and H. B. Smith and R. L. Dewar for valuable theoretical discussions. The authors are also grateful for the excellent technical support provided by S. Hyde and P. Alexander.

One of the authors (C.O.J.) acknowledges the financial support of Samsung Electronics, Korea during his stay at the Australian National University.

[1]R. W. Boswell, Phys. Lett. **33**, 457 (1970).
[2]R. W. Boswell, Plasma Phys. **10**, 1147 (1984).
[3]F. F. Chen, Plasma Phys. Controlled Fusion **33**, 339 (1991).
[4]A. R. Ellingboe, R. W. Boswell, J. P. Booth, and N. Sadeghi, Phys. Plasmas **2**, 1807 (1995).
[5]M. Light, I. D. Sudit, and D. Arnush, Phys. Plasmas **2**, 4094 (1995).
[6]P. K. Loewenhardt, B. D. Blackwell, R. W. Boswell, G. D. Conway, and S. M. Hamberger, Phys. Rev. Lett. **67**, 2792 (1991).
[7]A. Komori, T. Shoji, K. Miyamoto, J. Kawai, and Y. Kawai, Phys. Fluids B **3**, 893 (1991).
[8]R. W. Boswell, Ph.D. thesis, Flinders University of South Australia, 1972.
[9]B. M. Harvey and C. N. Lashmore-Davies, Phys. Fluids B **5**, 3864 (1993).
[10]R. W. Boswell and R. K. Porteous, Appl. Phys. Lett. **50**, 1130 (1987).
[11]A. Ellingboe and R. Boswell, Phys. Plasmas **3**, 2797 (1996).
[12]G. G. Borg and R. C. Cross, Plasma Phys. Controlled Fusion **29**, 681 (1987).
[13]A. J. Perry, R. W. Boswell, and H. M. Persing, ''Modulation in potentials in a helicon plasma reactor, to be submitted for publication in J. Vac. Sci. Technol.
[14]R. C. Davidson, *Methods in Nonlinear Plasma Theory* (Academic, New York, 1971).
[15]I. J. Morey and R. W. Boswell, Phys. Fluids B, **1**, 1502 (1989).
[16]See National Information Service Document No. DE85004960 (B. McVey, Plasma Fusion Center, Massachusetts Institute of Technology, Report No. PFC/RR-84-12). Copies may be ordered from the National Technical Information Service, Springfield, Virginia 22161.
[17]T. Intrator, S. Meassick, J. Browning, R. Majeski, J. R. Ferron, and N. Hershkowitz, Nucl. Fusion **29**, 377 (1989).
[18]R. L. Dewar (private communication).